Geochemical Mechanisms in Terrestrial Carbon Sequestration

J. E. Amonette, J. A. Capp,[(a)] A. Lüttge,[(b)] D. R. Baer, and R. S. Arvidson[(b)]

Supported by DOE/OBER/Center for Carbon Sequestration in Terrestrial Ecosystems, BES-Geosciences.

(a) Associated Western Universities student.
(b) Rice University.

Concern over the potential climate changes associated with increasing levels of atmospheric CO_2 has focused new research on the pathways and processes that enhance C sequestration. In this report we summarize the research initiated this year on key aspects of organic- and inorganic-C sequestration processes in soils. We also describe our exploration of a new microscopic technique for imaging changes in mineral surface topography resulting from precipitation and dissolution reactions such as might occur during C-sequestration.

Formation of Humic Materials at Oxide Surfaces

Restoration of organic soil C to levels typical of pre-agricultural soils (as much as twice the current levels) can be a significant sink for atmospheric C over the next 20-50 years and thereby help stabilize atmospheric levels during the transition to non-fossil sources of energy. For example, an increase of 1 wt% C in the top 15 cm of a soil would sequester about 23 metric tons of C ha^{-1}. Whereas most of the C in soils is turned over quite rapidly by the activity of microbes, a small fraction can be retained in a recalcitrant form (i.e., humified) through the partial oxidation and polymerization of organic molecules such as hydroxybenzoic acids, amino acids, and polyphenols. Humification is believed to be catalyzed by phenol oxidase enzymes secreted by fungi (Martin and Haider 1969; Nelson et al. 1979) demonstrated this process by bubbling air through a mixture of tyrosinase (an oxidase extracted from mushrooms) and several of the organic monomers just listed. In the present work, we sought to determine the influence of other solid-phase oxidants, such as the common Fe(III) and Mn(IV) oxide minerals, on the humification process. If these minerals further catalyzed the humification reaction, then agricultural management practices that promote their formation in soils (e.g., fertilization with Fe and Mn) might increase the amounts of C sequestered by this process.

We prepared a mixture of organic monomers (2 mM orcinol, resorcinol, p-hydroxybenzoic acid, L-glycine, L-serine, and vanillic acid) in a 100 mM phosphate solution buffered at pH 6.5. Separate 1 mg/mL suspensions of goethite (α-FeOOH), hematite (α-Fe_2O_3), birnessite (γ-MnO_2), an Fe-rich smectite (Panther Creek bentonite), and tyrosinase were also prepared. To a series of 7.5 mL polystyrene 1 cm cuvettes, we added 3.5 mL of the buffered organic monomer solution, 1 mL of the mineral suspension, and 0.5 mL of the tyrosinase solution. The mineral treatments were run in duplicate. Solutions with 1 mL of H_2O added in place of the mineral suspension were also run as controls. Each cuvette was then capped and incubated at 22 °C while continuously bubbling the mixture with house air using a small tube passed through the cap. At selected intervals after mixing, the absorbance of the mixture in the cuvette was measured using an HP 8452 diode-array UV-Vis spectrometer. The change in absorbance at 486 nm was used to measure reaction progress.

The solid-phase oxidants all yielded increases in the apparent reaction rate and extent (Figure 3.13). In

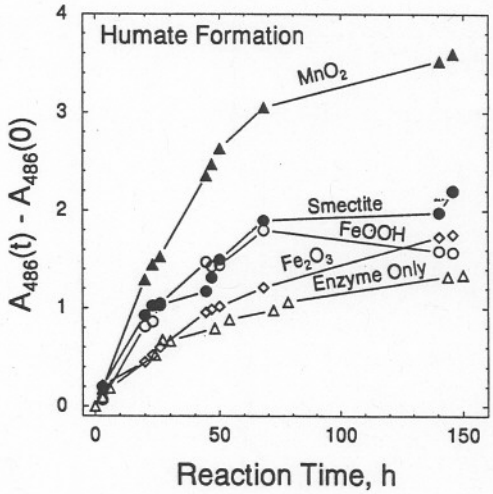

Figure 3.13. Rates of enzyme-catalyzed humification induced by Fe(III) and Mn(IV) mineral suspensions and by a solution containing no additional mineral oxidant.

general, the Fe(III)-bearing minerals increased the humification rate by as much as twofold, with smectite and goethite having a stronger effect than hematite. These results may stem from the greater surface area offered by the smectite (635 m^2g^{-1}) and goethite (87 m^2g^{-1}) than the hematite (6 m^2g^{-1}). The Mn(IV) oxide increased the humification rate by a factor of about 3. Although the surface area of the Mn(IV) oxide was not measured, it was certainly no more than that of the smectite, suggesting that the higher reduction potential of Mn(IV) ($E° = 1.20$ V) relative to Fe(III) ($E° = 0.77$ V) was the key factor in the higher humification rate.

These results suggest that the presence of Mn(IV) and Fe(III) minerals can aid the polymerization of humic materials in soils and that management practices that foster the presence of these minerals can have a significant impact on the overall rates of C sequestration achieved.

Stoichiometry of Calcite Precipitation

On a geologic time scale, precipitation of inorganic carbonate minerals is the main mechanism by which CO_2 has been removed from the atmosphere. At the pHs typical of the ocean and groundwater, the HCO_3^- ion is the dominant carbonate species in solution and the stoichiometry of the reaction can be written as

$$Ca^{2+} + 2HCO_3^- \rightarrow CaCO_3(s) + H_2O + CO_2(g) \quad (1)$$

This reaction implies that 1 mole of CO_2 is released to the atmosphere for each mole of $CaCO_3$ formed, suggesting that precipitation of carbonate invariably increases the short-term supply of atmospheric CO_2 (Schlesinger 1999). A simpler general form of the reaction can also be written in which no direct release of CO_2 is involved:

$$Ca^{2+} + HCO_3^- \rightarrow CaCO_3(s) + H^+ \quad (2)$$

Rather, precipitation of a mole of $CaCO_3$ consumes one mole of alkalinity (or creates one mole of acidity). The loss in alkalinity can come from the dissolved bicarbonate species to yield CO_2 as in the first reaction or from reaction with solid-phase pH buffers including organic matter and silicate minerals like plagioclase to yield other products as in:

$$NaAlSi_3O_8 + H^+ + 7H_2O \rightarrow Na^+ + Al(OH)_3 + 3H_4SiO_4 \quad (3)$$

As the pH-buffering capacity of soil solids is several orders of magnitude larger than that provided by groundwater species alone, it does not necessarily follow that one mole of CO_2 would be released for each mole of $CaCO_3$ that precipitates. The actual amount of CO_2 released will depend on the kinetics of the various possible pH-buffering reactions and the fluxes of water and gas through the soil. Furthermore, even in a strictly carbonate-buffered system, release of CO_2 in response to generation of H^+ would not be expected to be significant at pHs above about 8, due to the pK_1 of 6.35 for the carbonic acid-bicarbonate pair.

To demonstrate these points, we conducted experiments in which we measured the CO_2 released by $CaCO_3$ precipitation at a typical groundwater pH. As variables, we selected 1) the presence or absence of a solid-phase pH buffer (finely ground feldspar), and 2) the rate of removal of dissolved $CO_2(g)$ from the sample (headspace purging versus suspension sparging). Results of our most recent experiments are reported here.

The experimental apparatus consisted of two plastic gas-washing bottles connected in series that were continually flushed with a stream of CO_2-free $N_2(g)$ at about 32 $cm^3\ min^{-1}$. In one set of experiments, a sparging tube was immersed in the suspension. In the other set of experiments, the sparging tube was suspended above the suspension so that only the headspace was flushed, and CO_2 produced in the aqueous phase needed to diffuse to the gas-liquid surface to be collected in the $N_2(g)$ stream. The precipitation reactions were conducted in the first flask and the CO_2 evolved was trapped by 200 mL of 0.1 M NaOH in the second flask and subsequently measured by a total-C analyzer. Four apparatus were used simultaneously and purged with the same source of $N_2(g)$. The four reaction flasks initially contained 1 mmol of $NaHCO_3$ adjusted with HCl to pH 7.5 in a volume of 50 mL. Two flasks received an equivalent amount of $CaCl_2$, which was added by syringe after the gas flow had started, to yield a final volume of

100 mL; one of these flasks also contained 1 g of a powdered feldspar standard (NBS 99, <75 µm). The two remaining flasks also had final volumes of 100 mL and one of them contained 1 g of the feldspar. Thus, for a given experiment, $CaCO_3$ was precipitated in two apparatus, in the presence and absence of feldspar. Conditions in the other two apparatus served as $CaCO_3$-free controls. The pH of the reaction flasks was measured at the beginning and end of the precipitation experiments. In addition to CO_2 evolved during precipitation, a total C (C_T) balance was also made by acidifying the contents of the first flask to pH 2 at the end of the experiment and measuring the CO_2 evolved under the same sparging conditions. As flow rates varied slightly from one apparatus to the next, the C_T recovery data were used to normalize the data for CO_2 evolution during the precipitation. Experiments were conducted with reaction times of 16 or 64 h after addition of $CaCl_2$.

The results of these experiments yielded several insights into the stoichiometry of the $CaCO_3$ precipitation reaction. First, the final pHs varied with the type of gas flushing (solution or headspace, Figure 3.14). With solution sparging, the final pH in the $CaCO_3$ flasks increased from 7.5 to 7.8-7.9, as would be expected by removal of CO_2 from the system. With headspace flushing, the final pH in the $CaCO_3$ flasks decreased to final values of 7.3-7.4. With both gas-flushing systems, increases in pH to 8.3-8.9 were seen with the $CaCO_3$-free controls (data not shown).

Second, the presence of feldspar decreased the change in pH (Figure 3.14). That is, the feldspar buffered the pH of the solution closer to its initial value. The overall buffering capacity of the feldspar was low, however, as expected from the high solution:solid ratio employed.

Third, the net amounts of CO_2 evolved during $CaCO_3$ precipitation varied from essentially nil to as much as 23% of C_T (Figure 3.14). The maximum amount evolved, however, was slightly less than half the amount expected assuming the stoichiometry of the first equation and precipitation of all inorganic C as $CaCO_3$. With the exception of the lowest-pH data point, the amount of CO_2 evolved was inversely correlated (r^2 >0.999) with the final pH of the suspension. The outlying data point at pH 7.27

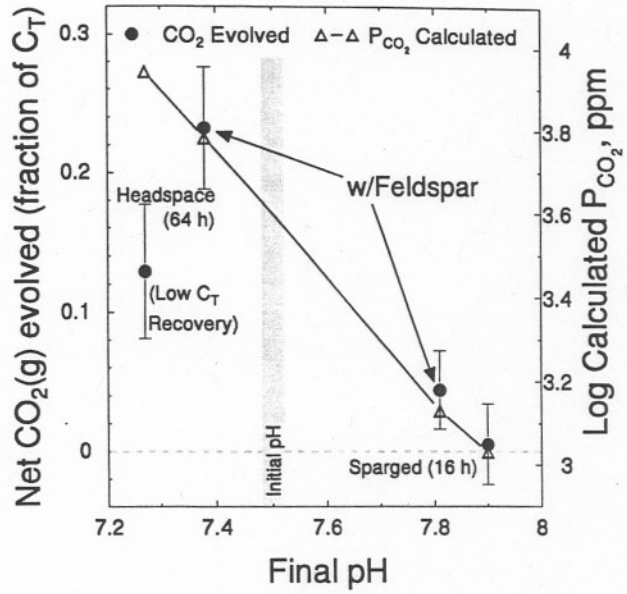

Figure 3.14. Net amounts of CO_2 evolved during $CaCO_3$ precipitation experiments (left axis) and calculated P_{CO2} in equilibrium with suspensions at final pH of experiments (right axis).

probably represents a leak in the gas flushing system as only 58% of the C_T was recovered during the acidification procedure for this sample. In all other samples, C_T recovery was 80-90%.

Taking the final pH values and the initial composition of each system as inputs to the MINTEQA2 thermodynamic speciation code (v 3.10, USEPA Environmental Research Laboratory, Athens, Georgia), we calculated the P_{CO2} in equilibrium with the precipitated $CaCO_3$ at the end of the experiment. A line with a negative slope of 1.47 is obtained when log P_{CO2} is plotted against pH, as expected from the equilibrium constant used in the calculation (Figure 3.14). What is striking, however, is the direct correspondence between the calculated P_{CO2} data and the evolved CO_2 data. These results suggest that each of the reactions had reached a steady state with respect to the P_{CO2} levels maintained in the reaction flask. Even though the systems are "open" in a thermodynamic sense, calcite is known to equilibrate rapidly with the surrounding fluid.

Thus, the primary factor influencing the calcite precipitation stoichiometry in these experiments seems to be the rate of gas removal and its influence

on the P_{CO2}. A secondary influence seems to be the degree of pH buffering by the solid phase. In all experiments where $CaCO_3$ was precipitated, the calculated steady-state P_{CO2} levels were higher than atmospheric levels (ca. 380 ppm). In soils and sediments, low gas exchange rates would tend to promote higher P_{CO2} levels, but this influence would be offset by the massive pH-buffering capacity of the solid phase, which is only hinted at in these experiments. For example, the solution:solid ratio in these experiments was 100, whereas in a typical groundwater, a ratio of about 0.3 would be expected. Ultimately, then, soil pH would control P_{CO2} and the amounts of CO_2 evolved during $CaCO_3$ precipitation.

In summary, our experiments suggest that the risk of CO_2 emission from $CaCO_3$ precipitation is inversely related to the pH maintained by a soil. At pHs above 7.9, little or no CO_2 evolution would occur. Extrapolation of the relation between CO_2 evolution and pH suggests that soils at pHs of about 6.8 or lower would stoichiometrically release 1 mole of CO_2 for each mole of $CaCO_3$ precipitated. From the standpoint of inorganic-C sequestration, the best soil management practices seem to be those that maintain soil pH > 7.9 and certainly no lower than 6.8. Further experimentation is under way to confirm and refine these observations.

Interferometric Microscopy of Calcite Surfaces

In the past decade, optical phase-shift interferometry has found increasing use in the topographical characterization of semiconductor and optic material surfaces (Onuma et al. 1994). Recent work at Yale University (Lüttge et al. 1999) has extended this technique to directly measure reactive surface area and dissolution rates of feldspar (abiotic) and apatite (microbial) ex situ. As applied by Lüttge and coworkers, the technique uses a closed-path Mirau double-beam interferometer objective attached to an optical microscope to measure the path length differences between white light reflected by the sample and light reflected by a reference surface. Transformation of the interferogram, which is collected in a matter of a second or two by moving the surface of the sample vertically using piezoelectric ceramics, results in a topographical map of the surface with absolute vertical resolution as small as a few nm and horizontal resolution of 1 um. Changes in the topography of the surface as a result of reaction can be monitored over time by masking part of the surface, which then serves as a reference for later measurements.

Key attributes of phase-shift interferometry (in addition to rapid data collection) are 1) the large depth of focus (100 um at nm-scale resolution, 1 mm at lower resolution), 2) the large field of view (up to 1 mm^2), and 3) the noninvasive nature of the technique. Because these attributes allow nm-scale information to be collected quickly on relatively large areas of rough surfaces, phase-shift interferometry is well-suited to the analysis of reaction rates on minerals and other heterogeneous surfaces having high environmental significance.

In our initial application of the technique, we examined the cleavage surface of calcite after cleaning and drying with ethanol. After this observation, we removed the specimen, which was mounted on a special orienting stub, subjected it to a 5-minute "etching" treatment with deionized H_2O, and remounted it in the instrument after drying the surface with ethanol. The spatial registration provided by the stub allowed us to easily find and examine the exact same portion of the specimen surface. We then let the specimen sit overnight in contact with humid air (typical of Houston in August) before examining it for a third time the next morning.

The results (Figure 3.15) clearly demonstrate the ease with which the calcite surface reconstructs itself. In Figure 3.15a, a deep etch pit located at the foot of a high terrace is shown along with a line indicating where a cross section of the pit was extracted. Numerous other shallow pits are also seen on the same level as the deep pit. The initial image of the deep pit taken after cleaning with ethanol yielded a cross section (Figure 3.15b) that was about 72 nm deep and 5.5 μm wide at the top. Immediately after etching with H_2O, the pit had enlarged to a 250-nm depth and a 7.3-μm width at the top (Figure 3.15c). However, upon equilibrating the surface overnight with humid air (Figure 3.15d), reconstruction of the calcite surface occurred to partly fill in the pit and eliminate the sharp features seen immediately after etching. The overall width at the top of the pit remained constant at about 7.3 μm.

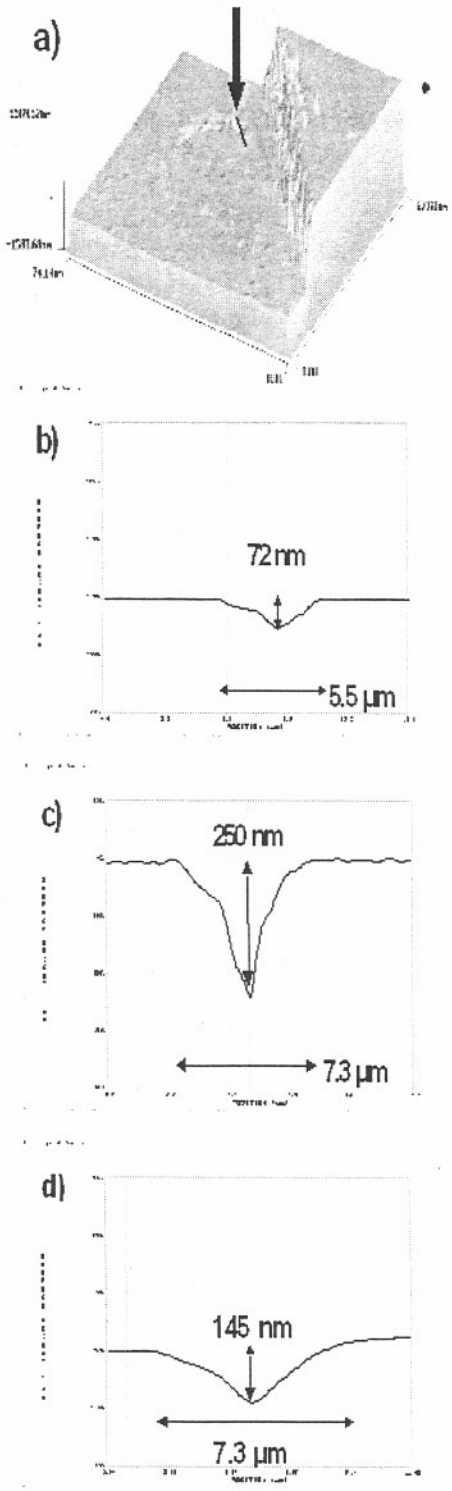

Figure 3.15. a) Interferometric microscope image of etch pit and step edge on calcite cleavage surface. Next three sections show cross sections of the pit (at arrow) measured b) before, c) immediately after, and d) 14-h after dissolution treatment with DI water.

Evidently the pit is located along a line defect perpendicular to the cleavage surface. The higher energy of sites located at this point cause it to dissolve more readily than the rest of the calcite surface. In humid air, however, the pit reconstructs to minimize the surface energy. Immediately after the etching process, the slopes of the sides of the pit are different (Figure 3.15c) yielding an asymmetric shape. This feature is well known from our atomic-force microscopy (AFM) studies and reflects the two main types of double-kink sites (obtuse and acute) exposed on the calcite surface (Liang et al. 1996). The ratio of the slopes is inversely proportional to the step velocity during the etching process.

This simple experiment demonstrates how interferometric microscopy can be used to collect information about dissolution and reconstruction processes on mineral surfaces. It is but a short step to apply the technique to the precipitation of coatings, whether organic or inorganic in nature, on mineral surfaces. In ongoing research, we are examining the impact of metal ions such as Mn^{2+} and Sr^{2+} on the calcite dissolution process to confirm earlier results we obtained with AFM (Lea et al. in review). Experiments examining the interactions of humic polymers with feldspar surfaces are also under way. These experiments should yield insights as to how attachment and polymerization of humics on the surface occurs and the degree to which it affects subsequent weathering of minerals to yield the alkalinity. Both of these mineral surface processes are key to the sequestration of atmospheric CO_2 by soils.

References

Lea, A. S., J. E. Amonette, D. R. Baer, and Y. Liang, *Geochim Cosmochim Acta* (in review).

Liang, Y., D. R. Baer, J. M. McCoy, J. E. Amonette, and J. P. LaFemina, *Geochim Cosmochim Acta*, **60**, 4883 (1996).

Lüttge, A., E. W. Bolton, and A. C. Lasaga, *Am. J. Sci.*, **299**, 1 (1999).

Martin, J. P., and K. Haider, *Soil Sci.*, **107**, 260, (1969).

Nelson, D. W., J. P. Martin, and J. O. Ervin, *Soil Sci. Soc. Am. J.*, **43**, 84 (1979).

Onuma, K., T. Karneyama, and K. Tsukamoto, *J. Crystal Growth*, **137**, 610 (1994).

Schlesinger, W. H., *Science*, **284**, 2095 (1999).